Polymer Chemistry

Accepted Manuscript

ROYAL SOCIETY OF CHEMISTRY

www.rsc.org/polymers

Graphical abstract

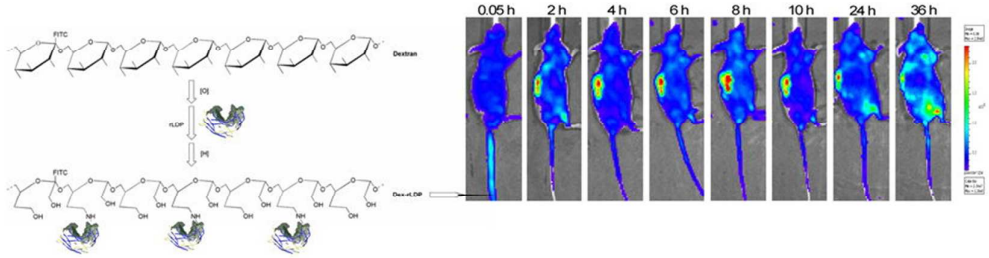

Cite this: DOI: 10.1039/c0xx00000x

www.rsc.org/xxxxxx

ARTICLE TYPE

A tumor-targeting dextran-apoprotein conjugate integrated with enediyne chromophore shows highly potent antitumor efficacy

Bin Li, Xiu-jun Liu, Liang Li, Sheng-hua Zhang, Yi Li, Dian-dong Li and Yong-su Zhen*

Received (in XXX, XXX) Xth XXXXXXXXX 20XX, Accepted Xth XXXXXXXXX 20XX
DOI: 10.1039/b000000x

A novel polymer-protein conjugate, Dex-rLDP, was prepared through conjugation of recombinant apoprotein (rLDP) of antitumor antibiotic lidamycin (LDM) to a macromolecular carrier dextran T40 with the periodate oxidation-hydroboron reduction method. Its structure was verified by means of SDS-PAGE, HPLC, FT-IR, CD and MOLDI-TOF MS. The weight-average molecular weight (M_w) of the glycoconjugate was 66.6 kDa determined by MOLDI-TOF MS, suggesting that approximately 3 mol of rLDP (MW 11.7 kDa) was attached per mole of oxidized dextran (M_w 32.1 kDa). Whereafter, the particle size, zeta potential and thermal stability of the dextranated conjugate were further characterized by TEM, DLS, and DSC. The DSC analysis revealed that dextranation could markedly enhance the thermal stability of the recombinant protein. To empower the conjugate with highly potent cytotoxicity, the resulting Dex-rLDP was then assembled with the active enediyne chromophoe (AE) of LDM to generate an enediyne-energized conjugate, namely Dex-rLDP-AE. *In vitro* MTT assay clearly indicated that the cytotoxicity of Dex-rLDP-AE was at least an order of magnitude higher than that of free LDM. At tolerable doses, Dex-rLDP-AE markedly suppressed the growth of human carcinoma xenografts and transplantable murine hepatoma. Notably, selective accumulation and retention of the fluorescently labeled Dex-rLDP within the tumor was detected by *in vivo* fluorescence imaging in tumor-bearing mice. The observed results indicate that this cross-linking strategy offers important implications for controlled and targeted drug delivery to solid tumors, and the enediyne-energized dextran-apoprotein conjugate is a potentially promising candidate for tumor targeted therapy.

Introduction

Lidamycin (LDM, originally named C-1027) is one of the most potent antitumor antibiotics that compose an active enediyne (AE) chromophore and a noncovalently bound apoprotein (LDP). In particular, AE and LDP can be dissociated and reconstituted in vitro.[1,2] LDM is now undergoing phase II clinical trials.[3] Recently, recombinant LDP (rLDP) whose biological activities was similar with that of native LDP had been successfully constructed and expressed in *E.coli* by our laboratory through recombinant DNA technology.[4] Results from tissue microarray showed that rLDP bound to various human tumors with significant difference from the corresponding normal tissues .[5]

In 1975, Helmut Ringsdorf presented his idea regarding the use of polymers as targetable drug carriers. Since then, polymer-drug conjugates (PDCs) have become a fast-growing field, and nearly a dozen such conjugates have come to the clinical trial stage.[6-8] Among these PDCs, poly(L-glutamic acid)-paclitaxel (PG-TXL, abbreviated as CT-2103) has advanced to Phase III clinical trials and is positioned to be the first of its class to reach the market.[9] One of the primary ways in which PDCs can increase the therapeutic index of anticancer agents is via the enhanced permeability and retention (EPR) effect, first described by Maeda *et al*. in 1986.[10] As reported, macromolecules larger than 40 kDa, as opposed to low molecular-weight compounds, do not extravasate through the capillaries of normal tissues. However, because of the impaired leaky vasculature and poor lymphatic drainage of solid tumors, they easily leak through the angiogenic capillaries in the tumors and accumulate within the tumor tissue.[7] This unique phenomenon in solid tumors is thus considered to be a landmark principle in tumor-targeting chemotherapy and is becoming an increasingly promising paradigm for anticancer drug development.[10]

Dextrans, which belong to the group of biodegradable natural polysaccharides, have been in clinical use for more than six decades for plasma volume expansion, peripheral flow promotion, and as antithrombolytic agents.[11] Owing to the excellent physico-chemical properties and physiological acceptance such as good biocompatibility, high stability and low toxicity, dextrans have been widely investigated in the recent decades as modification reagents to elevate drug solubility, stability, and half-life.[12-14] However, reports on the use of dextrans as carriers of PDCs (excluding from formulations) for

targeted drug delivery to tumors via the EPR effect were very limited.[15-16]

In an attempt to alter the tissue distribution and achieve selective delivery of the antitumor drug to solid tumors based on EPR effect, in the current studies we have designed and synthesized a tailor-made polymer-protein conjugate, Dex-rLDP, by covalently attaching recombinant lidamycin apoprotein (rLDP) to 40 kDa polymeric dextran with the periodate oxidation-hydroboron reduction method. The dextranated conjugate Dex-rLDP was characterized by various analytical methods and then assembled with the enediyne chomophore AE derived from LDM to form an enediyne-energized analogue Dex-rLDP-AE. *In vitro* cytotoxic activity of Dex-rLDP-AE against three cell lines was evaluated by MTT assay and *in vivo* antitumor efficacy was assessed with three tumor models. Furthermore, we studied the real time distribution and tumor localization of fluorescently labeled dextran-based conjugate for the first time by means of direct visual *in vivo* fluorescence imaging technique.

Experimental section

Materials

The engineered *E.coli* strain BL21 (DE3) that expressed rLDP, highly purified lidamycin and enediyne chromophore were kept in our laboratory. Dextran T-40 with a weight-average molecular weight (M_w) of 40 kDa was obtained from GE Healthcare (Uppsala, Sweden). Fluorescein isothiocynante-dextran T-40 (FD-40), 5(6)-Carboxyfluorescein N-hydroxysuccinimide ester (CFSE) and 3-(4,5-dimethylthiazol-2-yl)-2,5-diphenyltetrazolium bromide (MTT) were purchased from Sigma-Aldrich (St. Louis, MO). Isopropyl β-D-1-thiogalactopyranoside (IPTG) was product of Takara Biotechnology (Dalian, China). Modified RPMI-1640 and Dulbecco's modified Eagle's medium (DMEM) were from Thermo Fisher Scientific (Waltham, MA). Fetal bovine serum (FBS) was supplied by Life Technologies (Carlsbad, CA).

Preparation of enediyne-energized conjugate Dex-rLDP-AE

One liter of Luria-Bertani (LB) medium supplemented with 50 mg/mL kanamycin was inoculated with 50 mL of a starter culture that contained overnight culture of rLDP expressing strains. The inoculated medium was then maintained at 37 ºC with shaking at 220 rpm, and protein expression was induced with IPTG (0.1 mM final concentration) at an optical density at 600 nm ($OD_{600\ nm}$) of 1.0. After 8 h of induction, strains were harvested by centrifugation, and the periplasmic fractions of the collected strains were prepared with the osmotic shock method and purified with Ni^{2+} affinity column.[17] About 79 mg of purified rLDP was recovered from 1 L culture.

The purified rLDP was coupled to dextran as described previously with some alterations.[18,19] In a typical preparation, to 1.0 g (approximate 6.2 mmol glucose subunits) of dextran T-40 in 40 mL of distilled water was added 4.0 g (1.5 × 2 × 6.2 mmol, 2 mol of $NaIO_4$ was consumed per mol of glucose subunit) of $NaIO_4$ for complete oxidation of dextran. The mixture was allowed to stir for 20 h at 4 ºC in the dark and the excess $NaIO_4$ was removed by repeated ultrafiltration using a centrifugal filter with MWCO 3 kDa (Merck Millipore, MA, USA), followed by lyophilized with an Alpha 1-4 LD Plus freeze dryer (Martin Christ, Germany) to give 0.7 g of dialdehyde dextran.

Next, 20 mg (0.6 μmol) of freeze-dried dialdehyde dextran was added to a 3 mL stirred solution (0.1 M $NaHCO_3$, pH 8.5) containing 5-fold excess of rLDP (35 mg, 3.0 μmol) at 4 ºC in the dark for 12 h. The resulting mixture was then reduced with 17 mg (0.4 mmol) of $NaBH_4$ for an additional 2 h. After ultrafiltration, aliquots of the reduced solution were repeatedly applied to size-exclusion high performance liquid chromatography (SE-HPLC) on a TSK G2000SW_{XL} gel filtration column (7.8 mm × 300 mm, 5 μm particle size) (Tosoh, Tokyo, Japan) to remove excess rLDP. The fractions containing the dextran-modified rLDP were pooled, desalted and lyophilized to afford the desired Dex-rLDP conjugate (21.8 mg) as fluffy white floccules.

The enediyne-energized analogue Dex-rLDP-AE was prepared by assembling AE molecule derived from LDM into Dex-rLDP in PBS buffer as previously described and reversed-phase HPLC equipped with a Jupiter 300A C_4 column (4.6 mm × 250 mm，5 μm particle size) (Phenomenex, Torrance, CA, USA) was used to examine the enediyne-energized process.[20]

Characterization of Dex-rLDP

The degree of conjugation of Dex-rLDP was determined by matrix-assisted laser desorption/ionization time-of-flight mass spectrometry (MALDI-TOF MS). A drop of rLDP or Dex-rLDP solution was mixed with an equal volume of 2, 5-dihydroxybenzoic acid (DHB) matrix solution and allowed to dry on a stainless steel plate prior to MALDI analysis on an Axima CRF plus (Shimadzu, Tokyo, Japan) or UltrafleXtreme instrument (Bruker Daltonics, MA, USA). The number of mole of rLDP attached to one mol of dialdehyde dextran was then calculated by taking into account the molecular masses of dialdehyde dextran and Dex-rLDP. IR spectra were recorded in the 4000-400 cm^{-1} regions by the FT-IR microscope transmission method on a Nicolet 5700 FT-IR spectrophotometer (Thermo Fisher Scientific, Waltham, MA, USA). Circular dichroism (CD) spectra were recorded at room temperature utilizing a J-815 Circular Dichroism spectropolarimeter (Jasco, Tokyo, Japan) with a cell path length of 1 mm. The concentrations of rLDP and Dex-rLDP were all 1 mg/mL (0.1%, w/v). Transmission electron microscopy (TEM) was employed to observe the morphology of the prepared conjugate. A drop of the Dex-rLDP solution at a concentration of 1 mg/mL (0.1%, w/v) was mounted onto a carbon-coated grid and negatively stained with aqueous 1% uranyl acetate, followed by removing the excess fluid with a filter paper. Then the grid was allowed to dry and visualize using a JEM-1400 Plus transmission electron microscope (JEOL, Tokyo, Japan) equipped with a Quemesa CCD camera with an accelerating voltage of 80 kV. The size and zeta potential of rLDP and Dex-rLDP were collected by dynamic light scatting (DLS) using a ZetaPlus analyzer (Brookhaven, NY, USA). Dex-rLDP was prepared for DLS by dilution with physiological saline to a final concentration of 2 mg/mL (0.2%, w/v) followed by sonication for 60 s. For size and size distribution measurement, the scattering angle was set as 90º. To evaluate the stability of the conjugate, differential scanning calorimetry (DSC) analysis was performed using a DSC1 thermal analyzer (Mettler-Toledo, Zürich, Switzerland) with a programmed heating rate of 10

ºC/min over a temperature range of 30 to 200 ºC. Freeze-dried solid specimens (Approximately 2 mg) were heated in sealed aluminum pans.

Cell culture and *in vitro* cell viability assay

The human ovarian carcinoma cell lines SK-OV-3 and OVCAR-3 were grown in modified RPMI-1640 and the human epidermoid squamous carcinoma cell line A431 in DMEM. All culture medium were supplemented with 10% heat-inactivated FBS, penicillin G (100 U/mL) and streptomycin (100 μg/mL), and all cell lines were maintained in a humidified incubator which provided an atmosphere of 5% CO_2 at a constant temperature of 37 ºC.

The *in vitro* cell growth inhibitory activity of the free drug DOX and conjugate against these cell lines was evaluated by MTT assay. In brief, cells were seeded for replicates of three onto 96-well plates at a density of 4,000 cells per well and cultured overnight with culture medium then treated with different concentrations of drug solution. The cells were incubated for 48 h and then treated with MTT solution (5 mg/mL). After another 4 h of incubation, the supernatant was discarded and 150 μL of DMSO was added to each well to dissolve the formazan crystals. The absorbance of the resulting solution was recorded at 570 nm by using a Multiskan MK3 microplate reader (Thermo Fisher Scientific, MA, USA). Cell viability was calculated as a percentage of the untreated controls.

Experimental animals and tumor models

Six to eight week-old female BALB/c athymic nude mice and Kunming mice, weighing 20 ± 2 g, were purchased from Vital River Laboratories (Beijing, China). Animals were housed in individual cages on a 12 h light-dark cycle with free access to standard laboratory mouse chow and water. All animal protocols were in accordance to the guidelines of the Institutional Animal Care and Use Committee.

The subcutaneous human epidermoid carcinoma A431 and human lung carcinoma H460 tumor xenograft models were established using tumor tissue block. Mice were inoculated subcutaneously (s.c.) with exponentially growing carcinoma cell suspension (2×10^6/mouse). Tumors were allowed to grow for 3 weeks, aseptically cut into pieces about 2 mm^3 in size, and transplanted s.c. by a trocar needle into the right flanks of nude mice. The subcutaneous murine hepatoma H22 tumor homograft model was established by injecting of hepatoma H22 cells passaged in the ascites form (2×10^6/mouse) into the right oxter of each Kunming mice.

Localization of the fluorescein-labeled conjugate by *in vivo* and *ex vivo* optical fluorescence imaging

Attachment of rLDP to dextran made no free amino group left to introduce the fluorescent probe. Thus, fluorescein-labeled dextran T-40 (FD-40) was chosen and then conjugated with rLDP using the above described conjugation method. Mealwhile, free rLDP was labeled by a fluorescein molecular CFSE according to our previously reported method.[21]

Tumor localization was investigated in A431 tumor-bearing mice. First, fluorescently labeled Dex-rLDP (F-Dex-rLDP) and its control, F-rLDP were injected into the tail veins of mice (n = 2) at the dose of 20 mg/kg body weight when the solid tumors reach a volume of about 100 mm^3. Next, the mice were anesthetized by isofluorane at several selected time points (0.05, 2, 4, 6, 8, 12, 24 and 36h) after injection and placed in the imaging chamber of the IVIS-200 optical imaging system (Xenogen, Alameda, CA, USA). Then the fluorescence images were taken by the built-in thermoelectrically cooled CCD camera and processed with living image software. At 36 h, all of the animals were euthanized and sacrificed, and the tumors and major organs were excised for *ex vivo* fluorescence imaging with the same procedure.

In vivo antitumor efficacy

The potential tolerated dose of Dex-rLDP-AE was first assessed in A431 tumor-bearing nude mice. When tumors reach a volume ranging from 80 to 100 mm^3, mice were randomly divided into 3 groups (n = 6). One of the groups received no treatment served as blank control. The remaining 2 groups were injected once with 200 μL of two different dosages of Dex-rLDP-AE (0.4 and 0.7 mg/kg) via the lateral tail veins, respectively. Tumor size was measured every 3 days using vernier calliper and tumor volumes were calculated using the following formula: V (mm^3) = $1/2 \times a^2 \times b$, where a and b represented the short and the orthogonal long diameters of the tumor, respectively.

The subsequent experiment was done in nude mice bearing H460 xenografts. In this case, mice were randomized (n = 6) and treated with Dex-rLDP (20 mg/kg), LDM (0.05 mg/kg, the approximate maximum tolerated dose in nude mice) and four different dosages of Dex-rLDP-AE (0.05, 0.1, 0.2 and 0.3 mg/kg). All mice in treatment groups were treated weekly for a total of 2 weeks (qw × 2). At the humane endpoint, mice were sacrificed, tumors were removed and weighed, and the tumor growth inhibition (TGI) for each group was calculated. For histological examination, specimens taken from various organs were fixed in 10% formalin and embedded in paraffin, and then paraffin sections were stained with hematoxylin and eosin (H&E). To further confirm the antitumor efficacy of Dex-rLDP-AE, this experiment was also carried out in Kunming mice bearing H22 homografts. In the H22 model, the number of mice was 10 for each group, and treatment started 1 day after tumor implantation.

Statistical Analysis

Statistical analysis was performed using Graphpad Prism 5 software. Statistical significance was assessed by the Student's t-test, and P values less than 0.05 were considered to be statistically significant.

Results and discussion

Preparation and purification of Dex-rLDP-AE

A primary question in the preclinical development of dextran-drug conjugates is which molecular weight of dextran should be selected for the conjugation since dextrans are aviliable commercially as different molecular weights. In a previous study using fluorescein-labeled dextrans (FDs), Mehvar *et al.*

demonstrated that, in rats, higher molecular weight dextrans were prone to accumulated in the liver while lower molecular weight dextrans were easy to rapidly eliminate from the kidney.[11,22] Later, Dreher *et al.* found that Dextrans with molecular weights between 40 and 70 kDa had the highest accumulation in solid tumors.[23] Thus, in this present study we selected dextran T-40 for clinical use as the macromolecular carrier. After comparison of the numerous synthesis methods reported by Takakura *et al*.,[24] we subsequently utilized the periodate oxidation method for dextran activation. To determine the optimum reaction conditions, the influence of the degree of oxidation of dextran, the molar ratio of dialdehyde dextran to rLDP and reaction time were investigated (data not shown). Preliminary studies showed that the optimized conditions (dextran oxidized to 100%, the molar ratio of rLDP to dialdehyde dextran of 5:1, reaction time 12 h) resulted in a desirable yield of Dex-rLDP by the periodate oxidation-hydroboron reduction method.

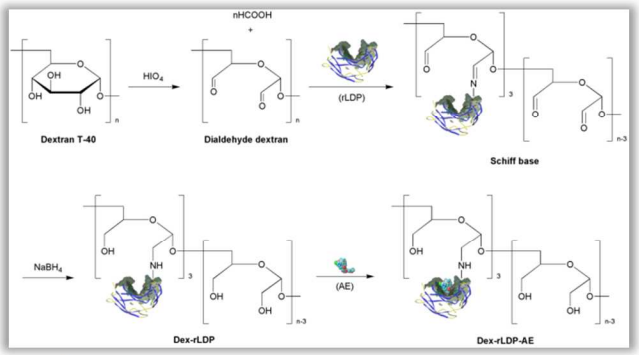

Fig.1 The schematic representation of the preparation process of Dex-rLDP-AE.

The preparation of the polymer-conjugated macromolecule, Dex-rLDP, involved oxidation, condensation and reduction reactions (Fig. 1). Firstly, the hexose rings of dextran were cleaved by periodate oxidation and the two aldehyde groups were introduced at the C-2 and C-4 positions of the glucose subunits. Then the free amino groups of rLDP condensed with dialdehyde dextran to form the Schiff base. The imine bonds as well as the remaining aldehyde groups of this base were subsequently reduced using hydroboron reduction to obtain the glycoconjugate Dex-rLDP because of the instability of the imine bond and the abnormal pharmacokinetics of dextran-based conjugates which contained reactive aldehyde groups.[18] Additionally, reduction could prevent further binding of the rest aldehyde groups to proteins and body components *in vivo*.[25]

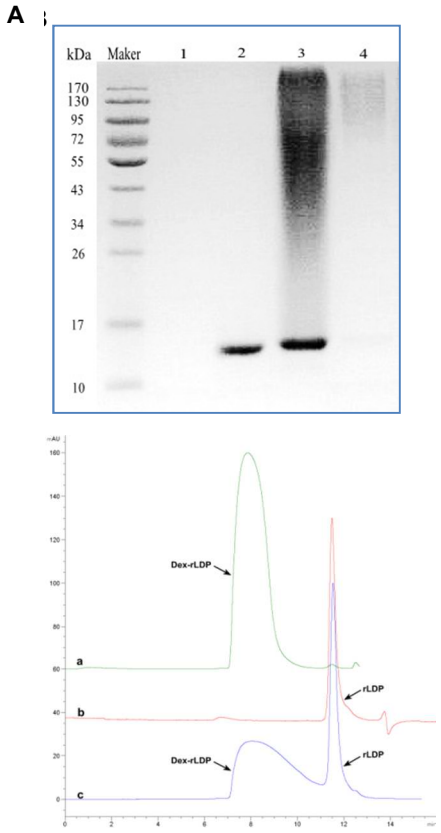

Fig.2 The elution profiles of Dex-rLDP (a), rLDP (b) and the crude product after reaction for 12 h (c). SE-HPLC analysis was performed on a TSK G2000SW$_{XL}$ column at ambient temperature. The mobile phase was 50 mM sodium phosphate (pH 6.8) with a flow rate of 0.8 ml/min and detection wavelength at 280 nm. (B) SDS-PAGE analysis of dialdehyde dextran (lane 1), rLDP (lane 2), the crude reaction product after reaction for 12 h (lane 3) and purified Dex-rLDP (lane 4).

Figure 2A (lower panel) showed the separation of Dex-rLDP and unreacted rLDP by gel filtration chromatography. The sharp elution peak presented in the elution profile (retention time t_R = 11.5 min) was attributed to unconjugated rLDP, whereas the new broad peak appeared in the early elution position (t_R = 8.0 mim) indicated that rLDP had been covalently linked to dextran. The content of the broad peak (Fig. 2A, upper panel) was confirmed by SDS-PAGE analysis (Fig. 2B), where a diffuse band with increasing molecular weights was observed. The causes of this band was possibly due to the relatively broad molecular weight distribution of reactant dextran T-40 resulting in the polydispersity of the conjugate.

To obtain a potent cytotoxicity, AE dissociated from LDM in methanol was eventually reassembled with Dex-rLDP in PBS and then purified using centrifugal filter. The presence of the characteristic absorbance at about 350 nm of AE in RP-HPLC indicated that the successfully assembly of Dex-rLDP with AE (Fig. S3).[20] Based on the peak-area of the chromophore (AE), the assembly rate of the AE with the LDP-containing Dex-rLDP was 74%.[26]

Characterizations of Dex-rLDP

The characterizations of macromolecular Dex-rLDP were summeried in Table 1. Firstly, the positive-ion MOLDI-TOF MS for Dex-rLDP and rLDP was carried out to determine the degree of the prepared conjugation. Recombinant protein rLDP was a *E.coli*-expressed $(His)_6$-tagged protein. MOLDI-TOF MS analysis (Fig. S2) showed that the molecule weight of this purified protein (98% purity determined by SEC-HPLC, see Fig. 2A, middle panel) was 11,693 Da, in consistent with the SDS-PAGE electrophoresis result (Fig. 2B, lane 2 and Fig. S1). Nevertheless, after reaction with dextran, the peak appeared at around *m/z* 66,562 (Fig. S2), which further revealed successful conjugation. According to the experimental results and the theoretical M_w of 32,110 Da for dialdehyde dextran, the calculated values of rLDP component are 34,562 Da resulting in average three molecules of rLDP conjugated with the oxidized dextran. On the basis of the MS analysis, the proposed molecular structure for the conjugate was outlined in Figure 1.

Table 1. The physicochemical behaviors of Dex-rLDP.

Analytical method	Results
UV-vis (λ_{max})	280 nm
HPLC (t_R)	7.9 min
MOLDI-TOF MS (*m/z*)	66562
FT-IR (ν_{max})	3296, 2945, 1646, 1538, 1454, 1401, 1342, 1239, 1134, 1048, 841, 660 cm^{-1}
CD (Negative bands)	210, 220 nm
TEM (Diameter)	20 ~ 50 nm
DLS (Mean Size; Zeta potential)	27.2 nm; -0.34 mV
DSC (Denaturation temperature)	undetected

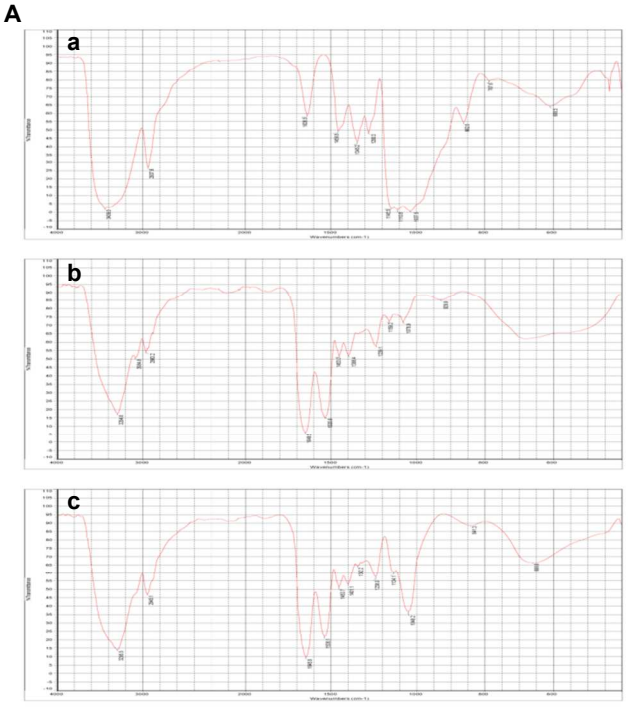

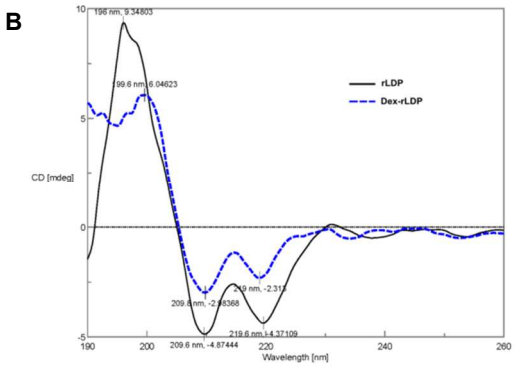

Fig 3. (A) IR spectra of dialdehyde dextran (a), rLDP (b) and Dex-rLDP (c). (B) CD spectra of rLDP and Dex-rLDP.

In a structural study, the FT-IR spectra (Fig. 3A) of Dex-rLDP are similar to that of rLDP except a new band at 1408 cm^{-1} that was believed to be the typical characteristic peak of polysaccharide,[27] which again validated the structure of the conjugate. Additionally, Dex-rLDP was shown to have similar CD spectral features (Fig. 3B) to that of unreacted rLDP, indicating that the process of conjugation had no significant effect on the structural property of the rLDP molecule during conjugation.

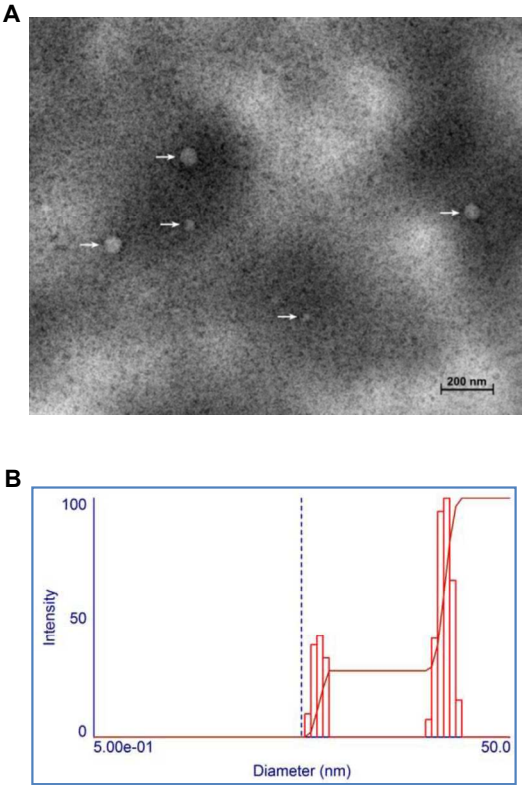

Fig 4. (A) The morphology of Dex-rLDP after negative staining with uranyl acetate. (B) The size distribution of Dex-rLDP.

To examine the surface morphology, Dex-rLDP was first negatively stained and then visualized using TEM as shown in Figure 4A. The prepared Dex-rLDP was found to be spherical, and the diameter ranged from 20 nm to 50 nm, which basically matched the result obtained by DLS (Fig. 4B), and was deemed to favor the EPR effect.[28,29] This size seemed to be reasonable

because the diameter of rLDP (Fig. S4) and the reported dextran T-40 was also at this nanoscale and was slight smaller than that of our synthesized conjugate.[11] Apart from the size and size distribution, the zeta potential was also determined by DLS, showing weak negative charge (-0.34 mV), which was considered to be favorable to the plasma and tissue disposition. This was because negatively and neutral charged conjugates reportedly had slower elimination and lower hepatic uptake, and can avoid the strong interaction with serum proteins, biological membranes and the uptake by macrophages in the circulation system.[11,29,30]

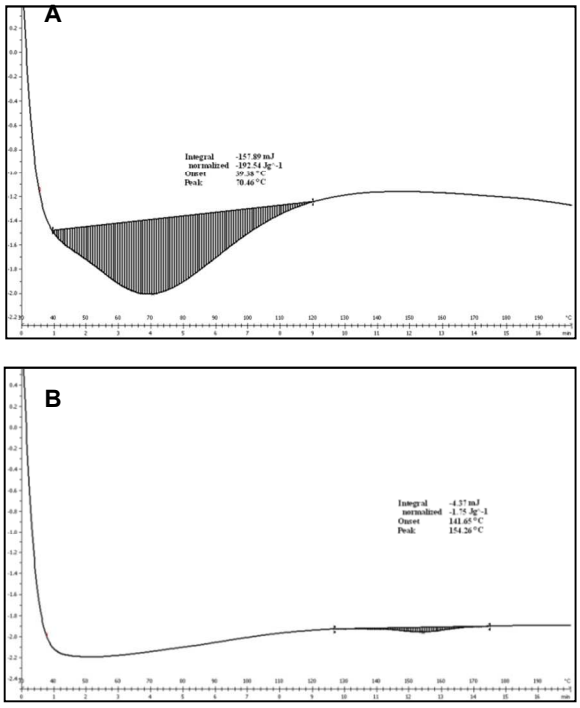

Fig 5. The DSC thermograms of rLDP (A) and Dex-rLDP (B).

Thermal stability of Dex-rLDP was evaluated with DSC. As can be seen from the DSC thermograms of rLDP and Dex-rLDP shown in Figure 5, before conjugation, rLDP displayed an intense peak near 70 ºC which belonged to the typical endothermic denaturation temperature of proteins caused by heating,[31] whereas in the case of Dex-rLDP, it appeared as almost a flat line, indicating that the thermal stability of rLDP was markedly enhanced after conjugation with dextran. bottom right). Similar observation was also reported by Zhu *et al.*.[32] The enhanced thermal stability could be attributed to the increase in molecular weight of Dex-rLDP according to the the published report.[31]

In vitro cytotoxic activity

Cytotoxic activity of LDM and Dex-rLDP-AE against three different types of cell lines was determined using MTT assay. As shown in Table 2, both showed highly potent growth inhibitory effects judged from their half inhibitory concentrations (IC_{50}), whereas it was noticed that the cytotoxic activity of Dex-rLDP-AE increased obviously compared with LDM. The free LDM showed an IC_{50} ranging from 0.04 to 6.1 nM, while the IC_{50} values (ranged from 0.003 to 0.4 nM) obtained for the synthesized conjugate was found to be 14-73 times lower than that of LDM.

Table 2. IC_{50} values of LDM and Dex-rLDP-AE against three human carcinoma cell lines after 48 h exposure.

cell lines	IC_{50} (nM)	
	LDM	Dex-rLDP-AE
SK-OV-3	0.365	0.005
OVCAR-3	0.042	0.003
A431	6.105	0.357

The enhanced cytotoxicity with respect to Dex-rLDP-AE could be accounted for the relatively high content of AE in the conjugate compared with the AE of LDM control sample since more than one molecule of rLDP attachment to per molecule dextran carrier. Moreover, the presence of dextran might enhance the penetration of drugs into a tissue-like matrix and improves the drugs transport inside the cells by macropinocytosis process.[33,34]

Tumor localization and accumulation

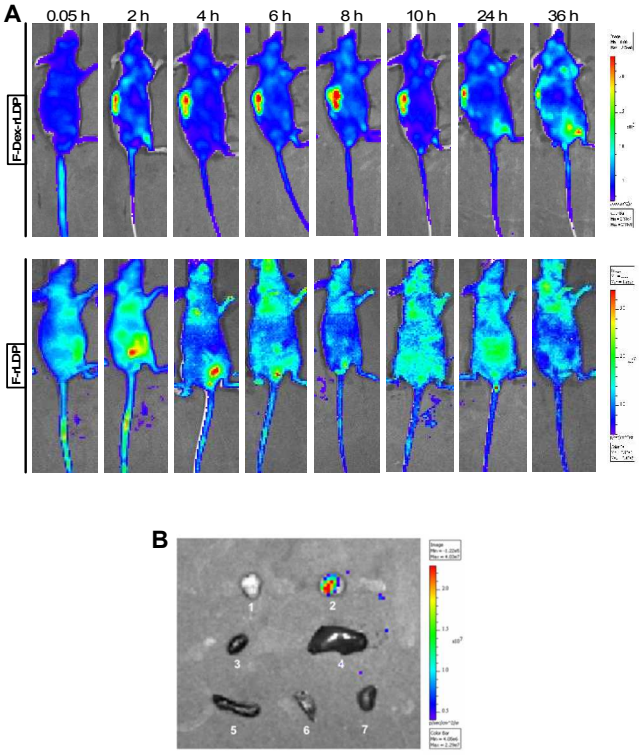

Fig 6. (A) Representative *in vivo* fluorescence images of epidermoid carcinoma A431 xenograft bearing nude mice at appointed times after tail vein injection of F-Dex-rLDP or its control, F-rLDP. (B) *Ex vivo* fluorescence images of the excised tumor (1) from the lower mouse in (A), and the excised tumor (2), heart (3), liver (4), spleen (5), lung (6) and kidney (7) from the upper mouse in (A). Mice were sacrificed at the end of the *in vivo* fluorescence imaging (36 h post-injection).

To confirm the EPR effect, tumor localization and accumulation of Dex-rLDP were carried out *in vivo* imaging in A431 tumor-bearing mice. This method allowed us to obtain visualized tumor localization and accumulation of drugs. As shown in Figure 6A, most of the F-rLDP was rapidly cleared from the body at around 6 h after administration and no obvious accumulation was observed in the tumor all the time. In contrast,

in the case of the macromolecular conjugate, the fluorescence signal of F-Dex-rLDP inside the tumor region began to emerge appreciably at about 2 h and remained at a higher level until 36 h before it slowly declined, suggesting that the macromolecular conjugate Dex-rLDP can selectively and continuously accumulate in the tumor site. Subsequently, the tumor and major organs were excised and imaged. As Figure 6B revealed, F-Dex-rLDP still exhibited relatively obvious fluorescence signal in the excised tumor rather in comparison with that of F-rLDP. More importantly, there was no detectable signal observed in excised normal organs of mice treated with F-Dex-rLDP, which further confirmed the targeting specificity of Dex-rLDP.

The improved disposition properties of macromolecular Dex-rLDP could be partly attributed to its decreased permeation through the glomerular capillary wall according to the earlier pharmacokinetic study of dextran conjugates reported by Takakura *et al*. and Zhao *et al*. since molecular weight is the most important determinant in glomerular filtration of the macromolecule.[30,35] Apart from a decrease in glomerular filtration rate, for tumor-bearing mice, another more reasonable explanation was that the EPR effect, a unique phenomenon of solid tumors related to their anatomical and pathophysiological differences from normal tissues, resulted in the remarkable tumor accumulation and slower tumor clearance.[10] The EPR effect referred to the enhanced permeability and retention effect of macromolecules with molecular weight above 40 kDa in solid tumors, resulting from a combination of the increased permeability of tumor blood vessels and the decreased rate of clearance caused by the lack of functional lymphatic vessels in the tumor.[23] In the current study, coupling of rLDP to a widely used polymer, dextran, has significantly altered its molecular weight and therefore it is expected to selectively leak out from tumor vessels and accumulate in tumor tissues for a long period of time exploiting the EPR effect.

Therapeutic efficacy against human tumor xenografts in nude mice

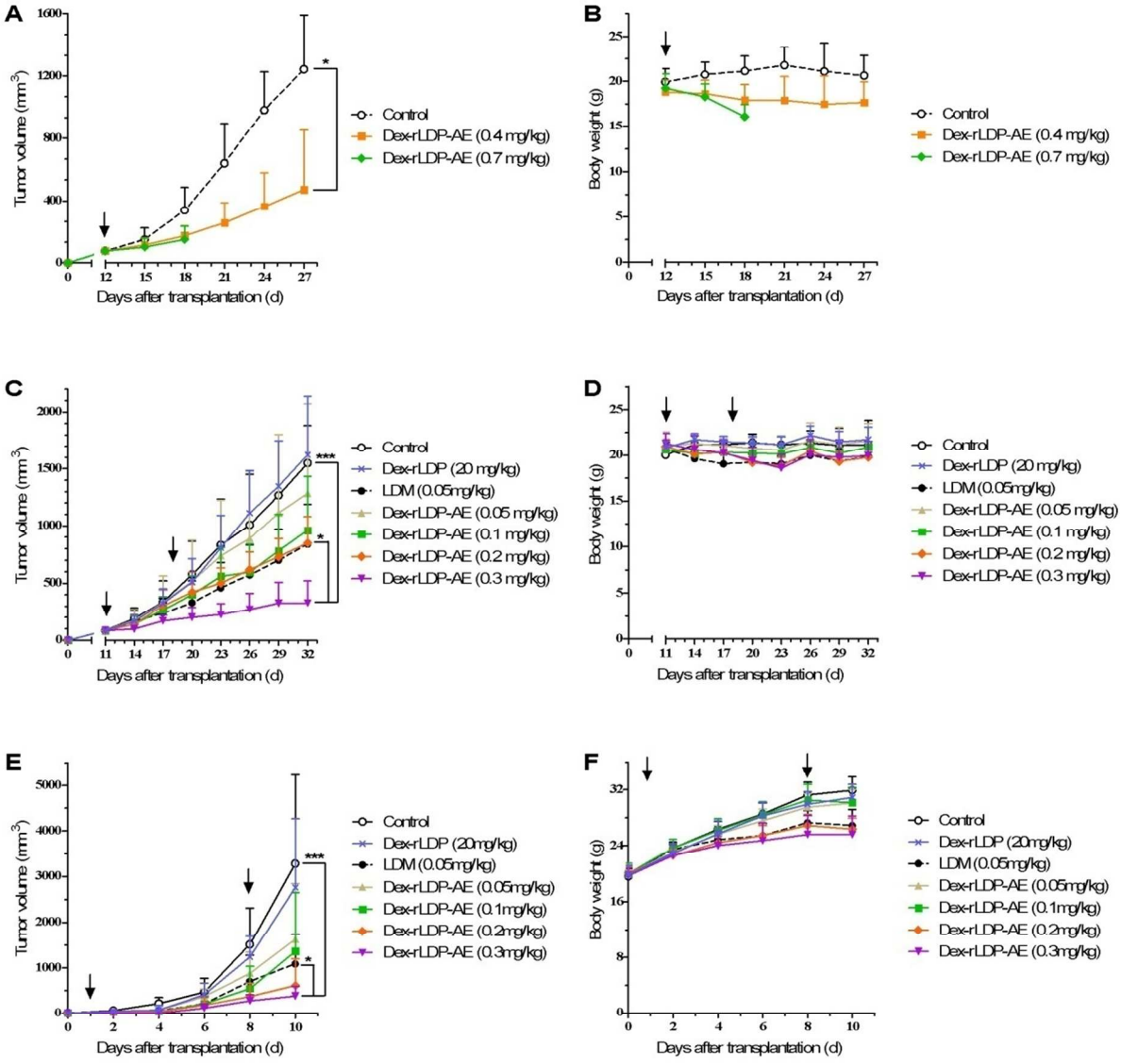

Fig 7. *In vivo* antitumor therapy of Dex-rLDP-AE on transplanted tumor models. Changes in tumor volume and body weight of human epidermoid carcinoma A431 xenograft-bearing mice (A and B, $n = 6$), human lung carcinoma H460 xenograft-bearing mice (C and D, $n = 6$) and murine hepatoma H22 homograft-bearing mice (E and F, $n = 10$) after treatment, respectively. (*P < 0.05 and ***P < 0.001 by the Student's *t*-test). Arrows denote the days of injection.

To determine the following administration schedules, two different doses (0.4 and 0.7 mg/kg) of Dex-rLDP-AE were administered to A431 xenograft-bearing nude mice. As shown in Figure 7B, there was a noticeable decrease in body weight in the group received with high-dose Dex-rLDP-AE (0.7 mg/kg) and three mice died 9, 12 and 13 days after injection, respectively. However, the body weight loss in mice treated with Dex-rLDP-AE at 0.4 mg/kg was less than 10% and no death was found. This allowed us to conclude that the maximum tolerated dose of Dex-rLDP-AE in nude mice lied in between 0.4 and 0.7 mg/kg. Meanwhile, it meant that a single administration of Dex-rLDP-AE could also effectively inhibit A431 tumor growth by 62.6% (Fig. 7A).

In view of that, there is much keratinized and necrotic substance inside the A431 tumor (Fig. S5), which might impede Dex-rLDP-AE exerting its full potential,[10,36] we employed H460 xenograft-bearing nude mice for the following experiment. The maximum dose of Dex-rLDP-AE was set to 0.3 mg/kg, and mice were treated on a schedule of qw × 2 according to the above results. As displayed in Fig. 8C, in this xenograft model, Dex-rLDP-AE exhibited an obvious dose-dependent tumor inhibition activity (Fig. 7C, Table 3 and Fig. S6). Moreover, the high-dose of Dex-rLDP-AE (0.3 mg/kg) was found to inhibit tumor growth most efficiently after the second treatment, with a tumor growth inhibition (TGI) of 75.1% ($p < 0.01$ versus LDM (45.7%)). Besides, there was no significant body weight loss or deaths in the Dex-rLDP-AE-treated groups compared with the control (Fig. 7D). These trends were in accordance with those observed on the homograft H22 tumor model (Fig. 7E and 7F). By histopathological examination, no toxicity related changes were found in the heart, liver, spleen, lung, kidney and intestine of mice treated with Dex-rLDP-AE (Fig. 8). The presented results suggested that dextranation could potentially enhance the antitumor efficacy of LDM, and could be well explained by the targeted and sustained accumulation of the macromolecular conjugate Dex-rLDP-AE in the tumor site, through the EPR effect, demonstrated by the above real-time fluorescence imaging technique. It means that this conjugate can stay in tumor tissues for a prolonged time, thus exerting better antitumor efficacy at tolerable doses.

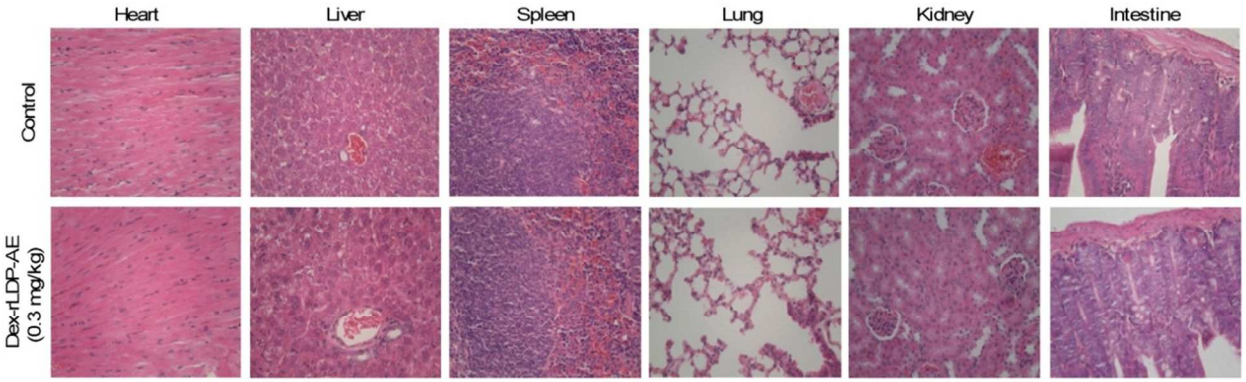

Fig 8. Histopathological examination of various organs (H & E staining, ×400) of lung carcinoma H460 xenograft-bearing mice treated with Dex-rLDP-AE. at dosage of 0.3 mg/kg. No toxicopathological changes were found in the heart, liver, spleen, lung, kidney and intestine.

Table 3. Antitumor activity of Dex-rLDP-AE in lung carcinoma H460 xenograft-bearing mice.

Groups	Dosage (mg/kg)	Mean tumor weight (g)	TGI (%)[a]
Control	-	0.84±0.20	-
LDM	0.05	0.45±0.18	45.7
Dex-rLDP-AE	0.05	0.72±0.50	14.0
	0.1	0.52±0.25	37.5
	0.2	0.46±0.08	44.8
	0.3	0.21±0.19	75.1[b]
Dex-rLDP	20	0.90±0.35	0

[a] TGI (Tumor growth inhibition) = (Wcontrol-Wtreated)/Wcontrol.

[b] $p < 0.01$ versus LDM-treated group.

In addition, we found that the non-enediyne-energized conjugate, Dex-rLDP, due to absence of potent AE, even dosed at 20 mg/kg did not produce any meaningful antitumor activity and caused no body weight loss (Fig. 8C-8F), indicating that Dex-rLDP was safe and suitable as a scaffold.

Conclusions

In the current study, recombinant lidamycin proprotein (rLDP) was attached to activated dextran by a convenient method to form a novel polymer-protein conjugate (PDC), designated Dex-rLDP. The number of rLDP contained in its conjugate was determined to be around three molecules based on its weight-average molecular weight. It should be noted that conjugation of rLDP to dextran enabled the recombinant protein enhanced stability against temperature and targeted accumulation in the tumor site

of tumor-bearing mice over a period of around 34 hours. To the best of our knowledge, this is the first report of using tumor-bearing mice optical imaging to directly demonstrate the dextran-based tumor targeting via the EPR effect. Furthermore, when loaded with the active enediyne (AE) molecule derived from LDM, this conjugate gained extremely potent cytotoxicity judged from experimentally determined IC_{50} values and revealed superior antitumor efficacy and well tolerated at therapeutically effective dose levels in transplanted tumor models.

These experimental data indicate that the biodegradable dextran could serve as a carrier for targeted delivery of chemotherapeutic agents into solid tumors through the EPR effect, ultimately improving their therapeutic efficacies and minimizing systemic toxicity. Furthermore, the enediyne-energized dextran-apoprotein conjugate is promising as a targeted drug for cancer therapy.

Acknowledgements

This work was supported by grants from the National High-Tech Research and Development Program of China (No. 2012AA02A301) and "Significant new drug development" Science and Technology Major Projects of China (No. 2013ZX09102064)

Notes and references

Institute of Medicinal Biotechnology, Chinese Academy of Medical Sciences and Peking Union Medical College, Beijing 100050, China. Fax: +86 10 83131808; Tel.: +86 10 83158065; E-mail: zhenys@public.bta.net.cn.

† Electronic Supplementary Information (ESI) available: Supplementary · gures. See DOI: 10.1039/b000000x/

1 Y.J. Xu, D.D. Li and Y.S. Zhen, *Cancer Chemother. Pharmacol.*, 1990, **27**, 41–46.
2 T. Tanaka, S. Fukuda-Ishisaka, M. Hirama and T. Otani, *J. Mol. Biol.*, 2001, **309**, 267–283.
3 Xin C, Ye S, Ming Y, Shenghua Z, Qingfang M, Hongxing G, Xu S, Yuanfu X, Yuan Z, Dongmei F, Juanni L, Yingdai G, Lianfang J, Rongguang S, Zhenping Z, Jianxiang W, Tao C, Chunzheng Y, Dongsheng X and Yongsu Z, *Gene. Ther.*, 2010, **17**, 1234–1243.
4 Q. Ru, H.X. Chen, Y.B. Zheng, B.Y. Shang and Y.S. Zhen, *Chinese J. Antibiot.*, 2010, **35**, 265–269.
5 L. Cai, H.X. Chen, Q.F. Miao, S.Y. Wu, Y. Shang and Y.S. Zhen, *J. Biotechnol.*, 2009, 144, 142–150.
6 F.X. Liu, L.X. Feng, L. Zhang, X. Zhang and N. Zhang, *Int. J. Pharm.*, 2013, **451**, 41–49.
7 N. Larson and H. Ghandehari, *Chem. Mater.*, 2012, **24**, 840–853.
8 D. Polyak, A. Eldar-Boock, H. Baabur-Cohen and R. Satchi-Fainaro, *Polym. Adv. Technol.*, 2013, **24**, 777–790.
9 C. Li and S. Wallace, *Adv. Drug Deliv. Rev.*, 2008**, 60**, 886–898.
10 J. Fang, H. Nakamura and H. Maeda, *Adv. Drug Deliv. Rev.*, 2011, **63**, 136–151.
11 R. Mehvar, *J. Control. Release*, 2000, **69**, 1–25.
12 C. Larsen, *Adv. Drug Deliv. Rev.*, 1989, **3**, 103–154.
13 S.S. Dhaneshwar, M. Kandpal, N. Gairola and S.S. Kadam, *Ind. J. Pharm. Sci.*, 2006, **68**, 705–714.
14 J. Varshosaz, *Expert Opin. Drug Deliv.*, 2012, **9**, 509–523.
15 T. Nomura, A. Saikawa, S. Morita, T. Sakaeda Kakutani, F. Yamashita, K. Honda, Y. Takakura and M. Hashida, *J. Control. Release*, 1998, **52**, 239–252.
16 Y. Chau, R.F. Padera, N.M. Dang and R. Langer, *Int. J. Cancer*, 2006, **118**, 1519–1526.
17 X.F. Guo, X.F. Zhu, Y. Shang, S.H. Zhang and Y.S. Zhen, Clin. *Cancer Res.*, 2010, **16**, 2085–2094.
18 R. Fagnani, M.S. Hagan and R. Bartholomew, *Cancer Res.*, 1990, **50**, 3638–3645.
19 M. Altikatoglu, Y. Basaran, C. Arioz, A. Ogan and H. Kuzu, *Appl. Biochem. Biotechnol.*, 2010, **160**, 2187–2197.
20 G.S. Zhong, S.H. Zhang, Y. Li, X.J. Liu, R.J. Gao, Q.F. Miao and Y.S. Zhen, *Cancer Lett.*, 2010, **295**,124–133.
21 B. Li, Y.B. Zheng, D.D. Li and Y.S. Zhen, *J. Pharm. Sci.*, 2014, **103**, 1204–1213.
22 R. Mehvar, M.A. Robinson and J.M. Reynolds, *J. Pharm. Sci.*, 1994, **83**, 1495–1499.
23 M.R. Dreher, W. Liu, C.R. Michelich, M.W. Dewhirst, F. Yuan and A. Chilkoti, *J. Natl. Cancer Inst.*, 2006, **98**, 335–344.
24 Y. Takakura, Y. Kaneko, T. Fujita, M. Hashida, H. Maeda and H. Sezaki, *J. Pharm. Sci.*, 1989, **78**, 117–121.
25 A.J. Domb, G. Linden, I. Polacheck and S. Benita, *J. Polymer Sci.*, 1996, **34**, 1229–1236.
26 G.S. Zhong, X.F. Guo, S.H. Zhang and Y.S. Zhen, *Biomed. Environ. Sci.*, 2011, **24**, 602-607.
27 C. Zhou, W. Gao, G. Lu, J. Ding, X. Wu, X. Huang, J. Chen, M. Liu, J. Jiang and H. Wu, *Carbohydr. Polym.*, 2013, **96**, 156–162.
28 S. Mitra, U. Gaur, P.C. Ghosh and A.N. Maitra, *J. Control. Release*, 2001, **74**, 317–323.
29 Y. Yang, D. Pan, K. Luo, L. Li and Z. Gu, *Biomaterials*, 2013, **34**, 8430–8443.
30 Y. Takakura, T. Fujita, M. Hashida and H. Sezaki, *Pharm. Res.*, 1990, **7**, 339–346.
31 S. Kim and A. Cavaco-Paulo, *Appl. Microbiol. Biotechnol.*, 2012, **93**, 585–600.
32 D. Zhu, S. Damodaran and J.A. Lucey, *J. Agric. Food Chem.*, 2010, **58**, 2988–2994.
33 W. Dang, O.M. Colvin, H. Brem and W.M. Saltzman, *Cancer Res.*, 1994, **54**, 1729–1735.
34 Vittorio, G. Cirillo, F. Iemma, G. Di Turi, E. Jacchetti, M. Curcio, S. Barbuti, N. Funel, O.I. Parisi, F. Puoci and N. Picci, *Pharm. Res.*, 2012, **29**, 2601–2614.
35 Q. Zhao, V. Tolmachev, J. Carlsson, H. Lundqvist, J. Sundin, J.C. Janson and A. Sundni, *Bioconjug. Chem.*, 1999 **10**, 938–946.
36 H. Maeda, *J. Control. Release*, 2012, **164**, 138–144.